Ninth International Conference on CFD in the Minerals and Process Industries
CSIRO, Melbourne, Australia
10-12 December 2012

MODELLING FILM DRAINAGE OF A BUBBLE HITTING AND BOUNCING OFF A SURFACE

Rogerio MANICA[1*], Evert KLASEBOER[1], Raghvendra GUPTA[1], Maurice H.W. HENDRIX[2,3], Claus-Dieter OHL[3] and Derek Y.C. CHAN[1,4]

[1] Institute of High Performance Computing, Singapore, 138632

[2] Physics of Fluids, University of Twente, P.O. Box 217, 7500 AE Enschede, The Netherlands

[3] Nanyang Technological University, Singapore, 637371

[4] Department of Mathematics and Statistics, The University of Melbourne, VIC 3010, Australia
*Corresponding author, E-mail address: manicar@ihpc.a-star.edu.sg

ABSTRACT

A theoretical model assuming lubrication theory has been developed for the interaction of bubbles rising under gravity against a glass plate. This system provides modelling challenges due to large deformations and widely different length scales where bubbles of micrometre to millimetre size form films that are on the nanometre range. Numerical simulations agree well with experimental data and reveal the interplay between surface tension, surface forces and hydrodynamic effects. The experimental data were obtained using two synchronised high-speed cameras to visualise both the bubble rise and bounce from the side and the thin film drainage from the top. In our numerical model, we assume the tangentially immobile hydrodynamic boundary condition at the air-water interface, which provides the best agreement when compared to experimental data all the way to film rupture. The reason for this counterintuitive result is attributed to small amounts of surface-active materials that are present in the water and would move to the interface rendering it immobile. The use of thin film theory is still accurate if the film Reynolds number is smaller than unity.

NOMENCLATURE

$\mathbf{u}$	velocity vector	R	radius of the bubble
p	pressure	h	separation
σ	interfacial tension	D	dimple size
ρ	density	r	radial coordinate
μ	viscosity	z	vertical coordinate
V	speed	τ	shear stress

INTRODUCTION

Interactions involving soft materials such as drops and bubbles in multiphase systems have applications in a wide variety of fields ranging from pharmaceuticals, detergents, water cleaning and mineral extraction. Modelling and numerical simulations of such systems present challenges that are not easy to overcome. Identifying the bubble interface and its deformation and movement can be done using numerical techniques such as the volume of fluid (VOF) or level-set. When a bubble is close to a surface or two bubbles are really close to each other such techniques require very refined grids and the computational time can become unreasonably large. On the other hand, the use of lubrication theory to model the last stages of thin film drainage can be used if the local Reynolds number of the system is smaller than unity.

Up until recently, experimental investigations of bouncing bubbles were restricted to side view recordings to observe deformations and bounces [Tsao and Koch, 1997; Malysa et al, 2005]. The interferometric technique had been widely used to observe film drainage, but experimental results were restricted to small deformations and low velocities [Derjaguin and Kussakov, 1939; Fisher et al, 1991; Klaseboer et al, 2000; Manica et al, 2010]. The development of high-speed cameras allows the study of much faster phenomena so that interferometric techniques can now be used to capture the evolution of fringes for systems at higher speeds and larger deformation [Hendrix et al, 2012].

In this work we use both numerical simulations and experimental data to analyse the interaction and bounce of a bubble rising under gravity against a flat glass surface. Numerical simulations are compared to the experimental data to infer information that is not directly available. The experiments are performed using two synchronised high-speed cameras. The first camera is used to observe and extract the position of the centre of mass as well as the shape of the bubble as it interacts and deforms while the second records the evolution of the thin film using an interferometric technique.

MODEL DESCRIPTION

Assuming that the continuous phase is a Newtonian fluid, the drainage can be modelled by the continuity and Navier-Stokes equations written as

$$\nabla \cdot \mathbf{u} = 0 \tag{1}$$

$$\rho\left(\frac{\partial \mathbf{u}}{\partial t} + \mathbf{u}\cdot\nabla\mathbf{u}\right) = -\nabla p + \mu\nabla^2\mathbf{u} + \mathbf{F} \tag{2}$$

where ρ is the density, μ dynamic viscosity, $\mathbf{u}$ velocity vector, p pressure and $\mathbf{F}$ an external force, in our case buoyancy.

For our modelling, we need to provide adequate boundary conditions at the air-water interface. To reach that goal, we look at the experimental terminal velocities, V_T of bubbles with radius R between 0.35 mm to 0.75 mm. In our experiment, these data correspond to Reynolds numbers, $Re = 2R\,\rho\,V_T/\,\mu$ in the range 60 to 230. The experiment is repeated for many bubbles, but only about

10 videos are fully analysed. The experimental velocities are compared to theoretical predictions from numerical simulations as well as empirical correlations.

We have used ANSYS Fluent to perform axisymmetric CFD simulations to calculate the drag force on a rigid spherical bubble in a uniform flow having the same velocity as the terminal velocity with no-slip or stress-free boundary conditions at the bubble interface. The numerical results for the no-slip boundary condition showed excellent agreement with experiments while the ones with stress-free condition are significantly different.

We also performed a balance of forces by treating the bubbles as spheres of radius R with the tangentially immobile boundary condition at the air-water interface. The buoyancy force

$$F_{buoy} = \frac{4\pi}{3}\rho R^3 g \tag{3}$$

can be balanced to the steady state hydrodynamic drag force

$$F_{drag} = \frac{1}{2}\rho V_T^2 (\pi R^2) C_D \tag{4}$$

where the drag coefficient C_D is a function of Reynolds number and g is the acceleration due to gravity. We use the Schiller-Naumann formula [Clift et al, 1978] for C_D that is valid for $Re < 800$ with an error of less than ±5%:

$$C_D = \frac{24}{\mathrm{Re}}(1 + 0.15\,\mathrm{Re}^{0.687}) \tag{5}$$

Combining equations (3) to (5) provides the terminal velocity as a function of bubble size.

In Figure 1 we show the terminal velocities extracted from the side view for the bubbles analysed (diamonds) and compare to the theory just described (solid line) and also to the CFD solution (squares) for no-slip boundary condition. Terminal velocities for bubbles in ultra pure water [Duineveld, 1995], where the stress-free boundary condition applies are plotted for the boundary element method (BEM) (circles) [Klaseboer et al, 2011] and CFD (triangles). The excellent agreement with the no-slip solution indicates that the air-water interface is tangentially immobile.

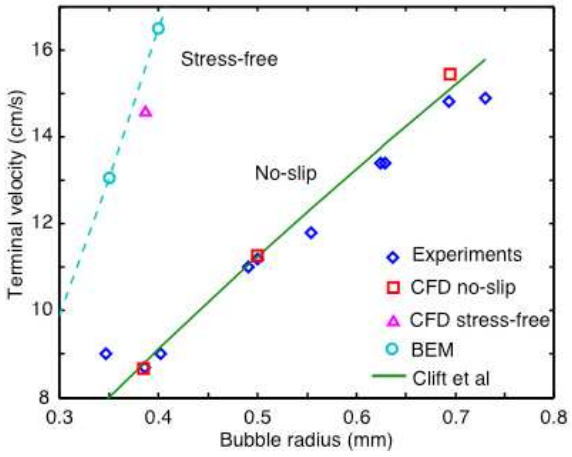

Figure 1. Terminal velocities for CFD simulations of axisymmetric flow around a spherical bubble with no-slip boundary condition (squares) compared to the balance of forces solution of Clift et al (solid line) and to experiments (diamonds). Results for the stress-free boundary condition are plotted for BEM (circles) and CFD (triangle).

Our system is characterised by two distinct Reynolds numbers: the global Reynolds number Re defined previously and the film Reynolds number Re_f defined as $Re_f = h_c\,\rho\,V_w/\mu$, where h_c is the film thickness at the centre of interaction and V_w is the maximum velocity of the water in the film. When the bubble is close to the glass plate a film forms and during the drainage stage, the film Reynolds number Re_f becomes small due to small separations and low velocities. Assuming that the problem remains axisymmetric, the Navier-Stokes and continuity equations can be simplified into the lubrication form

$$\frac{\partial p}{\partial r} = \mu\frac{\partial^2 u_r}{\partial z^2} \tag{6}$$

$$\frac{\partial p}{\partial z} = 0 \tag{7}$$

$$\frac{\partial u_z}{\partial z} = -\frac{1}{r}\frac{\partial (r u_r)}{\partial r} \tag{8}$$

where u_r and u_z are the velocity components in the r and z directions. In Figure 2, we define the theoretical quantities used in our model.

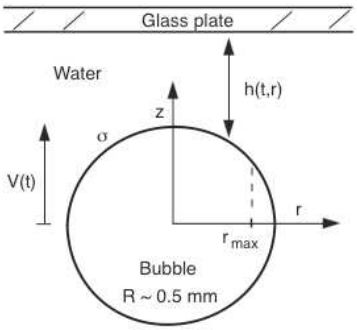

Figure 2. A bubble of radius R rises at velocity $V(t)$ against a glass plate in water. The variable $h(t,r)$ corresponds to the time-space separation between the bubble and the wall. The system is defined in axisymmetric form and solved from radial coordinate $r = 0$ to $r = r_{max}$, with $r_{max} < R$.

We start with the system of equations (6) to (8) and apply the no-slip boundary condition at the glass plate and the tangentially immobile boundary conditions at the air-water interface, an assumption well justified by the experimental results of terminal velocities plotted in Figure 1. After some algebraic manipulation, the Stokes-Reynolds model can be derived [Chan et al, 2011]

$$\frac{\partial h}{\partial t} = \frac{1}{12\mu r}\frac{\partial}{\partial r}\left(r\,h^3\frac{\partial p}{\partial r}\right) \tag{9}$$

The pressure is calculated by the Young-Laplace equation of the form [Chan et al, 2011]

$$\frac{\sigma}{r}\frac{\partial}{\partial r}\left(r\frac{\partial h}{\partial r}\right) = \frac{2\sigma}{R_L} - \Pi - p \tag{10}$$

where R_L is the Laplace radius ($R_L \sim R$), σ is the interfacial tension, p is the pressure in the film and $\prod$ is a surface force which is only relevant when the separation becomes really small (<0.1 µm) just before bubble adhesion.

We need one initial condition, which is defined as

$$h(0, r) = h_o + \frac{r^2}{2R} \qquad (11)$$

where h_o is the initial separation and time $t = 0$ is taken at a position where the bubble still rises at terminal velocity and the deformation due to the presence of the wall can be neglected.

We also need four boundary conditions. Due to symmetry $\partial p/\partial r = \partial h/\partial r = 0$ at $r = 0$. For the far-field boundary conditions we assume the pressure decays as $1/r^4$ [Yiantsios and Davis, 1990] to write $r\partial p/\partial r + 4p = 0$ at $r = r_{max}$. The last boundary condition assumes $dh/dt = V(t)$ at $r = r_{max}$ [Klaseboer et al, 2000]. In our simulations $V(t)$ is taken to be the velocity of movement of the centre of mass of the bubble from the experimental data. Another possibility is to calculate $V(t)$ through a balance of forces [Klaseboer et al, 2001].

EXPERIMENTAL

Experiments have been performed to confirm the numerical results. A schematic of the experimental apparatus together with photographs from the respective cameras is presented in Figure 3.

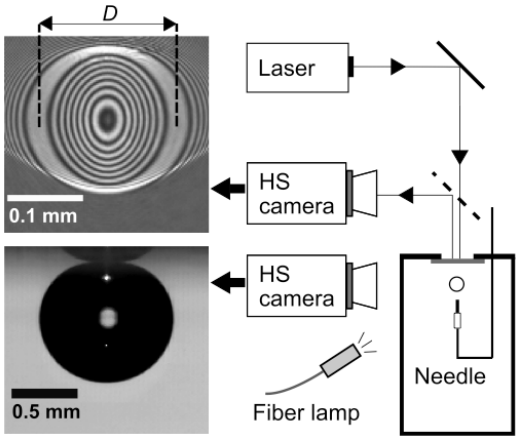

Figure 3. Experimental set up: A millimetre size bubble is released from a needle and rises under gravity against a glass surface. Two synchronised high-speed cameras capture the movement and shape of the rising bubble (bottom left photograph) and at the same time, the film drainage evolution through interferometry (top left image).

A typical experimental result is plotted in Figure 4. The top sequence shows the interferometric photographs at selected stages of interaction: bubble rising, dimple formation, film rupture and three-phase contact line expansion. We notice that while the film is continually changing, the corresponding side view images at the bottom sequence look mostly stationary.

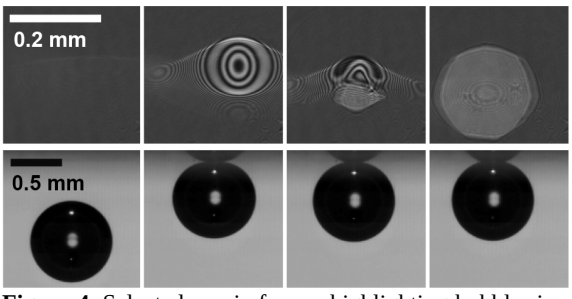

Figure 4. Selected movie frames highlighting bubble rise, interaction with the glass plate, film rupture and three-phase contact line formation. The top sequence corresponds to interferometric data from the top camera while bottom sequence represents side view images.

In Figure 5, we show a sequence of fringes where curvature inversion, also called dimple, and film drainage can be observed. These fringes are then converted to film profiles and analysed. Most of the numerical work presented in this manuscript involves this stage of interaction.

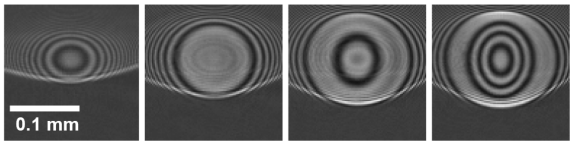

Figure 5. Typical sequence of interferometric fringes for time-step 0.37 ms between frames during the first contact of the bubble against the glass surface. The second frame shows flattening of the bubble surface while the third presents curvature inversion or dimple formation.

The experiment is repeated and movie files are collected for over 20 bubbles. We have analysed bubbles with small sizes to ascertain straight rise and axisymmetric drainage, at least during the initial phase of interaction.

RESULTS

In this section, we present comparisons between experiment and numerical simulations for a typical case. We have chosen a bubble radius $R = 385$ μm. This radius is small so that the bubble never fully detaches from the wall after the first contact. This allows the film drainage process to be known absolutely based on the point of film rupture. In all simulations we have used interfacial tension $\sigma = 72$ mN/m and water viscosity $\mu = 1$ mPa.s.

To obtain the film thickness $h(t,r)$, we use the Bragg equation for a fringe of order m: $h = m\,(\lambda/2\,n)$, where $\lambda = 532$ nm is the wavelength of the laser and $n = 1.33$ is the refractive index of water. In practical terms, the difference in separation between two white fringes is about 200 nm. Constructing the relative film profiles becomes an exercise of counting fringes. This process is performed using an automated routine in Matlab to identify changes in intensity for each movie frame. The absolute separation is obtained from the point of contact when the bubble has touched the wall. After that, we count backward to produce the time evolution of the bubble shape.

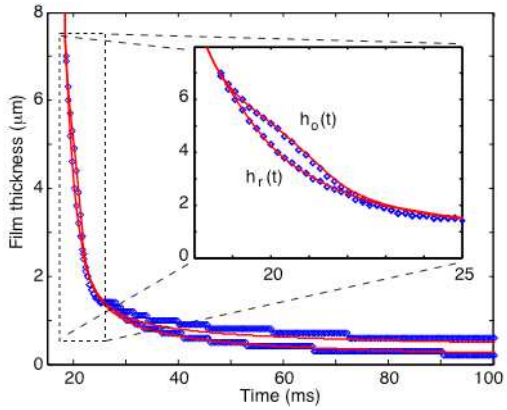

Figure 6. Evolution of the position at the centre $h_o(t)$ and at the rim $h_r(t)$ of the dimple during first contact and subsequent film drainage.

Results for drainage of the centre as well as rim of the dimple region are presented in Figure 6. The excellent agreement between experiments (symbols) and the numerical solution (solid lines) all the way to bubble attachment indicates that lubrication is still the main contribution during the interaction process once the film becomes thin enough. Notice that the first impact and dimple formation happens in about 5 ms while the slow drainage process takes over 200 ms. Any theoretical model that assumes bubble attachment at the moment of close contact would be an oversimplification.

A further test to our theory is the evolution of the bubble profile as the film drains. In Figure 7 we show the comparison between the numerical solution (solid lines) and experiment (symbols) during the first encounter between the bubble and the glass surface. This stage only comprises about 3 ms of the drainage process presented in Figure 6. Once again the agreement is excellent both in time and space without any adjustable parameters in the model. Note the curvature inversion and dimple formation. Any model that assumes that the film is flat would miss most of the physics.

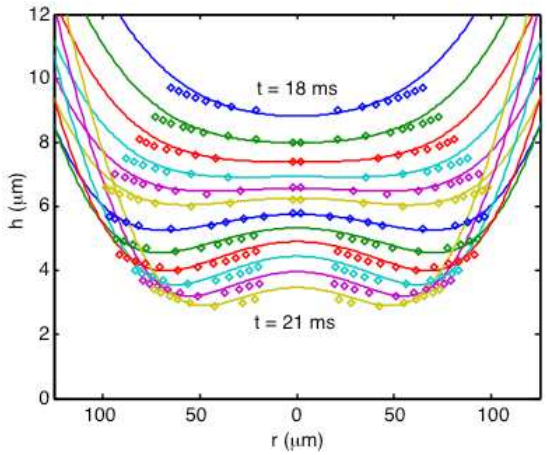

Figure 7. Spatiotemporal evolution of the bubble shape during first encounter corresponding to the inset of Figure 6 from time 18 to 21 ms. The domain size was taken to be r_{max} = 270 μm for a bubble radius of R = 385 μm.

We also learn from the numerical solution that though the outside of the bubble is already moving apart after one millisecond, the central part is still approaching. The curvature inversion, also called 'dimple', occurs at t = 19 ms in this case and is a result of the pressure in the film exceeding the internal pressure, also called the Laplace pressure, ($2\sigma/R$) of the bubble. This feature is clearly highlighted in Figure 8 where the pressure profiles for the same time instants as those of Figure 7 are plotted.

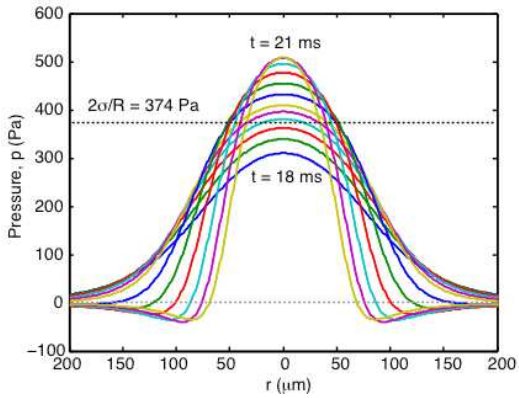

Figure 8. Pressure profiles corresponding to the same time instants as in Figure 7.

In Figure 9 we present the maximum water velocity as a function of radial position as the drainage evolves for the same time steps of Figure 7. For this case, the maximum outward velocity is reached before the first shown profile appears; the velocity decreases as the film becomes thinner. When the back of the bubble reverses from approach to retract the water has to occupy that space so that the velocity reverses from outward to inward. On the other hand, the central part of the bubble is still approaching. This interesting numerical result explains the 'suction' effect when we try to separate two bubbles. This effect is now known to be responsible for the coalescence of bubbles [Vakarelski et al, 2010] or drops [Bremond et al, 2008] when they are being separated from each other.

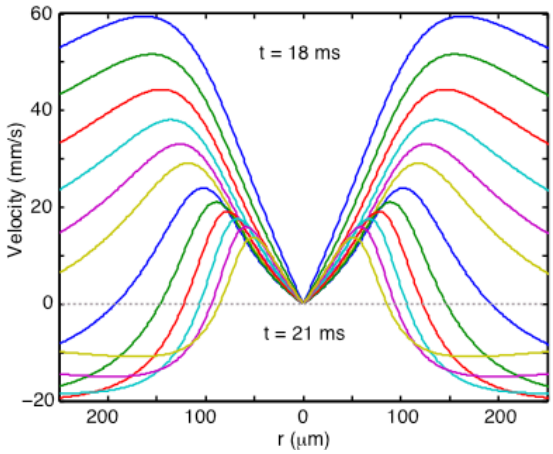

Figure 9. Maximum radial velocity of the water inside the film as time progresses where it is assumed the velocity profile is parabolic, consistent with the thin film solution.

The viscous shear stress can be calculated from [Klaseboer et al, 2000]

$$\tau = -\frac{h}{2}\frac{\partial p}{\partial r} \qquad (12)$$

In Figure 10 we present shear stress curves for the same time instants as shown in Figure 7. The shear stress values are relatively low due to deformation and are not enough to change the boundary condition at the bubble interface. It is interesting to notice that the maximum shear stress happens at the rim of the dimple and once again changes sign when the bubble surface starts to separate from the glass plate.

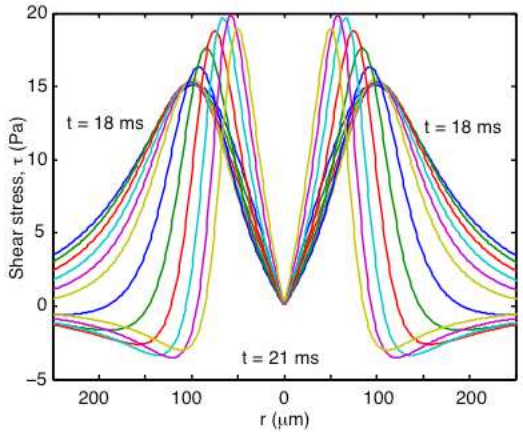

Figure 10. Shear stress curves for the same time instants as those of Figure 7 for times ranging from 18 to 21 ms.

To justify the validity of using lubrication theory for this system, we look at how the film Reynolds number changes as the drainage evolves. From Figure 11, we notice that it becomes smaller than unity before the first profile appears in Figure 7, even though the global Reynolds number is about 67. For larger bubbles the film Reynolds number would be above unity when dimple first forms and the model used in this work might not perform so well when compared to experiments.

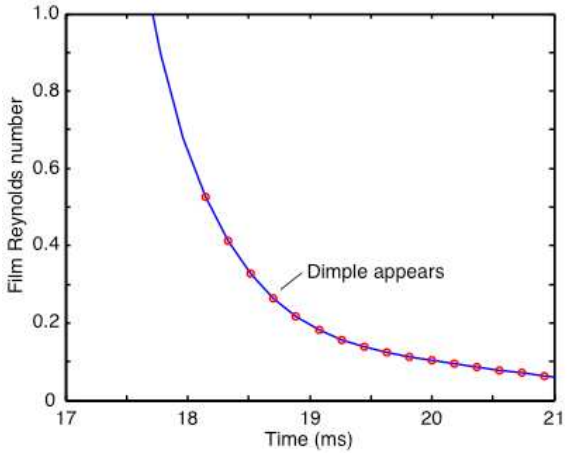

Figure 11. Film Reynolds number. Circles represent time instants that were plotted in Figure 7.

As stated before, the boundary condition applied at the air-liquid interface is of tangential immobility due to the presence of low concentration of surface-active impurities in the water that the shear stress is not able to compensate for. Earlier studies of bubbles in pure water [Duineveld, 1995] obtained terminal velocities of over 35 cm/s and those results were also confirmed by numerical solutions using a boundary element method [Klaseboer et al, 2011]. Our current experimental results attained velocities, which are less than half that value of about 15 cm/s for bubbles of the same size and compare well to experimental observations at small amount of known surfactant [Malysa et al, 2005].

CONCLUSION

In this work we have performed numerical simulations to model experimental data of a rising and bouncing bubble. The simulations allowed explaining a number of features that could not be captured directly by the experiment, for example the pressure profile, velocities and shear stresses. The use of synchronised high-speed cameras allowed observation of features that were not possible a few years back. The excellent agreement between numerical simulations and the experiment indicates that the model developed performs excellently when applied systems where a thin deformable film is present.

REFERENCES

TSAO, H.-K. and KOCH, D. L. (1997) "Observations of high Reynolds number bubbles interacting with a rigid wall," *Phys. Fluids* **9**, 44-56.

MALYSA, K., KRASOWSKA, M., and KRZAN, M., (2005) "Influence of surface active substances on bubble motion and collision with various interfaces", *Adv. Colloid Interface Sci*. **114-115**, 205-225.

DERJAGUIN B.V., and KUSSAKOV M. (1939) "Anomalous properties of thin polymolecular films" *Acta Physicochim URSS*, **10**, 26-45. Reprinted in *Prog. Surface Sci*.1992, **40**, 26-45.

FISHER L.R., HEWITT D., MITCHELL E.E., RALSTON J., and WOLFE J., (1992), "The drainage of an aqueous film between a solid plane and an air bubble" *Adv. Colloid Interface Sci*. **39**, 397-416.

KLASEBOER, E., CHEVAILLIER J.-Ph., GOURDON C. and MASBERNAT O. (2000), "Film drainage between colliding drops at constant approach velocity: Experiments and modeling" *J. Colloid Interface Sci*. **229**, 274-285.

MANICA, R., PARKINSON, L., RALSTON. J. and CHAN, D.Y.C. (2010) "Interpreting the Dynamic Interaction between a Very Small Rising Bubble and a Hydrophilic Titania Surface" *J. Phys. Chem. C*, **114**, 1942-1946.

HENDRIX, M.H.W., MANICA, R., KLASEBOER, E. CHAN, D.Y.C. and OHL, C.-D., (2012) "Spatiotemporal Evolution of Thin Liquid Films during Impact of Water Bubbles on Glasson a Micrometer to Nanometer Scale", *Phys. Rev. Lett.*, **108**, 247803.

CLIFT, R., GRACE, J. R. and WEBER, M. E., (1978), "*Bubbles, Drops and Particles"*, Academic Press, NY.

DUINEVELD, P.C., (1995) "The rise velocity and shape of bubbles in pure water at high Reynolds number", *J. Fluid Mech.*, **292**, 325-332.

KLASEBOER, E., MANICA, R., CHAN, D.Y.C. and KHOO, B.C. (2011) "BEM simulations of potential flow with viscous effects as applied to a rising bubble", *Eng. Anal. Bound. Elem*., **35**, 489-494.

CHAN D.Y.C., KLASEBOER E. and MANICA R. (2010), "Film drainage and coalescence between deformable drops and bubbles", *Soft Matter*, 7, 2235, 2264.

KLASEBOER, E., CHEVAILLIER J.-Ph., MATE, A., MASBERNAT O. and GOURDON C., (2001), "Model and experiments of a drop impinging on an immersed wall" *Phys. Fluids*, **13**, 45-57.

YIANTSIOS, S.G. and DAVIS. R.H. (1990), "On the buoyancy-driven motion of a drop towards a rigid surface or a deformable interface", *J. Fluid Mech*. **217**, 547-573.

VAKARELSKI, I.U., MANICA, R., TANG, X., O'SHEA, S.J., STEVENS, G.W., GRIESER, F, DAGASTINE, R.R. and CHAN, D.Y.C. (2010), "Dynamic interactions between microbubbles in water", *Proc. Nat. Acad. Sci*. **107**, 11177-11182.

BREMOND, N., THIAM, A.R., BIBETTE, J. (2008), "Decompressing emulsion droplets favors coalescence"

Phys. Rev. Lett. **100**, 024501.

